Modeling of clusters in a strong 248-nm laser field by a three-dimensional relativistic molecular dynamic model

G. M. Petrov,[1] J. Davis,[1] A. L. Velikovich,[1] P. C. Kepple,[1] A. Dasgupta,[1] R. W. Clark,[1] A. B. Borisov,[2] K. Boyer,[2] and C. K. Rhodes[2]

[1] *Plasma Physics Division, Naval Research Laboratory, 4555 Overlook Ave SW, Washington, DC 20375, USA*

[2] *Laboratory for X-Ray Microimaging and Bioinformatics, Department of Physics, University of Illinois at Chicago, Chicago, Illinois 60607-7059, USA*

(Received 2 September 2004; revised manuscript received 21 January 2005; published 25 March 2005)

A relativistic time-dependent three-dimensional particle simulation model has been developed to study the interaction of intense ultrashort KrF (248 nm) laser pulses with small Xe clusters. The trajectories of the electrons and ions are treated classically according to the relativistic equation of motion. The model has been applied to a different regime of ultrahigh intensities extending to 10^{21} W/cm^2. In particular, the behavior of the interaction with the clusters from intensities of $\sim 10^{15}$ W/cm^2 to intensities sufficient for a transition to the so-called "collective oscillation model" has been explored. At peak intensities below 10^{20} W/cm^2, all electrons are removed from the cluster and form a plasma. It is found that the "collective oscillation model" commences at intensities in excess of 10^{20} W/cm^2, the range that can be reached in stable relativistic channels. At these high intensities, the magnetic field has a profound effect on the shape and trajectory of the electron cloud. Specifically, the electrons are accelerated to relativistic velocities with energies exceeding 1 MeV in the direction of laser propagation and the magnetic field distorts the shape of the electron cloud to give the form of a pancake.

DOI: 10.1103/PhysRevE.71.036411 PACS number(s): 52.38.Ph

I. INTRODUCTION

The last several years have witnessed an explosion of activity involving the interaction of clusters [1–3] with intense ultrashort pulse lasers. Part of the reason for this interest in clusters is that the hot dense plasma created in the interaction with the laser can provide a compact source of x rays, incoherent as well as coherent radiation [4,5], and energetic ions. Some of the applications include euv lithography, euv and x-ray microscopy, x-ray tomography, nuclear fusion resulting from the generation of fast ions to drive a fusion reaction in a deuterium plasma, and a variety of applications in biology [4] and material sciences. The emitted x-ray radiation would also provide a useful tool as a backlighter for diagnosing dense plasmas. Even though gases are attractive for x-ray generation, they exhibit weak absorption of laser radiation and a corresponding low efficiency for conversion of the incident laser energy into x rays. Solid targets are likewise not particularly well suited to absorb laser radiation in the ultrashort pulse regime. However, solid targets can be designed to absorb increased laser energy for longer laser pulse durations and, under these conditions, can convert the incident energy into a high yield of incoherent x rays; the anticipated scenario for indirect drive fusion targets.

Conversely, atomic or molecular clusters are targets with unique properties. Possessing the properties of solids and gases, they combine the advantages of both. Clusters absorb much more energy compared to gases [6,7] and offer a flexibility in design [1] not found in solid targets. In essence, clusters can provide optimal conditions for laser energy absorption, the creation of ions with high charge, and coherent x-ray emission [1,4,5].

The recent literature is abundant with papers describing the evolution of large ($>10^5$ atoms) and small ($<10^3$ atoms) clusters irradiated by intense ultrashort pulse lasers. Among the most popular treatments is the so-called "nanoplasma model" [6], which treats the cluster as a miniature (few nm in size) high-density spherical plasma. This model describes the dynamics of ionization, electron heating, and cluster expansion, and assumes that the laser-cluster interaction occurs as a result of coupling through the so-called plasmon resonance. The electrical conductivity is represented by the Drude model with provisions to account for the resonance that occurs through the coincidence of the frequency of the incident laser wave with the plasma frequency [8]. An improvement of this picture includes the influence of electron-cluster surface collisions, achieved in Ref. [9], by the replacement of the plasma dielectric constant with an effective value for this quantity. Other models [10–13] have investigated harmonic generation and the oscillations of the electron cloud with respect to the immobile ions present inside the cluster that respond to the combined action of the laser field and the Coulomb interaction induced by the charge separation. In subsequent work, Milchberg and coworkers developed a one-dimensional hydrodynamic model of laser-cluster interactions [14,15]. Siedschlag and Rost developed a microscopic model for the interaction of small rare-gas clusters with soft x-ray radiation produced by a free electron laser [16]. Rose-Petruk *et al.* proposed the ionization-ignition model, in which the combined field of the laser and cluster ions leads to enhanced ionization producing ions with high charge states [17]. Smirnov and Krainov investigated a broad range of issues involving the laser cluster interaction and coupling extending from cluster formation to x-ray generation [18]. Schroeder *et al.* introduced the so-called "collective oscillation model" for small clusters (10–30 Å) [19,20]. These ordered motions of the outer elec-

trons, previously considered for single atoms [21–23], behave like a giant quasiparticle, hitting the cluster with an energy of tens of keV causing inner-shell ionization. Even though this picture explains some of the observations, it depends on assumptions that need to be proven in order to accurately represent the role of the outer electrons. Finally, a molecular dynamics model approach for modeling the cluster dynamics has been undertaken by Last and Jortner [24–26], Eloy *et al.* [27,28], and Taguchi *et al.* [29].

Mainly, the studies cited above implement spatially averaged fluid models. Recent findings in conjunction with other considerations, however, prompted us to adopt the molecular dynamics approach. For example, recent investigations strongly suggest that spatially averaged models provide poor, if not an utterly flawed, descriptions of the cluster dynamics [15]. Furthermore, one-dimensional models are appropriate only at sufficiently low laser intensities. As shown below, the problem is either two or three dimensional depending upon the peak laser intensity. The small number of particles ($10^3 - 10^5$) we are dealing with causes additional difficulties. The multidimensional nature of the problem computationally requires fine spatial resolution and a large number of grid points. This leads to just a few particles per elementary volume. In such situations, the validity of fluid models falls under suspicion.

We describe the laser-cluster interaction with a particle simulation model similar to that developed by Last and Jortner and focus specifically on the domain of high laser intensities; this is the regime in which relativistic effects and "collective oscillations" may become important. It has been established that this different ordered mode of ultraintense laser-cluster interactions commences at intensities in excess of 10^{20} W/cm^2, the range that can be reached in stable relativistic channels [30–37]. We note that as the intensity is raised, the magnetic field causes the configuration of the electron cloud to alter its shape from a sphere to a pancake and the combined action of the electric and magnetic fields accelerates the electrons to a relativistic velocity in the direction of propagation.

The objectives of the present paper are (i) the investigation and (ii) the description of the dynamics of small Xe clusters irradiated by a high intensity ultrashort pulses, and (iii) the determination of the conditions under which this model exhibits a transition to the "collective oscillation" picture [19,20]. We also evaluate the role played by the plasmon resonance energy during absorption [6].

II. MOLECULAR DYNAMICS MODEL

There are three principal types of particle simulation models: particle-particle (PP), particle-mesh (PM), and particle-particle-particle-mesh (PPPM) pictures [38]. The PM is the most widely used method for particle simulations, but unusual circumstances prompted us to give preference to the PP method. The main reason we selected the PP method is that we deal with a small system (several thousand particles) with long-range forces. Another reason to prefer the PP to the PM method is the three-dimensional (3D) nature of the analysis. The PP method can handle a 3D problem just as easily as a 2D treatment with insignificant (less than a factor of 2) increase in computational time, while the large number of grid points in a 3D geometry makes the PM method computationally disadvantageous compared to the PP approach. The PM method can handle only smoothly varying forces and requires high spatial resolution (smaller than the Debye length). Accordingly, to study the dynamics of clusters, we employed a relativistic time-dependent 3D particle-particle simulation model. This picture describes the interaction of an intense ($10^{17}-10^{21}$ W/cm^2) linearly polarized ultrashort 248-nm laser pulse (10–100 fs) with small Xe clusters (10–100 Å); it characterizes the details of the electron and ion motion and power absorption as the cluster evolves in time. The molecular dynamics model has two principal features, specifically, (i) the creation of particles (electrons and ions) and (ii) a description of their motion in space and time.

Initially, we discuss details of the ionization mechanisms and the creation of new particles. We assume that the electrons are created instantaneously through optical field ionization (OFI). At sufficiently high laser intensities, the ionization is predominantly due to OFI and the collisional ionization can be neglected. At sufficiently low intensities, where inelastic collision processes are important, the rate of collisional ionization can be calculated from the electron energy distribution function (EEDF) and included in the model. We take into account only one type of ion with an average charge $(Z-1)$ calculated from the relation [18]

$$\frac{1}{4Z}\left(\frac{I(Z)}{27.21}\right)^2 = \frac{E_0}{5.142\times 10^9}, \tag{1a}$$

$$E_0(t) = \sqrt{\frac{8\pi I_0(t)}{c}}, \tag{1b}$$

where E_0 is the slowly varying amplitude of the applied laser field in units (V/cm), I_0 is the laser intensity, c is the vacuum speed of light, and I(Z) is the ionization potential of $Xe^{(Z-1)+}$ in units (eV). At any given time $Z(t)$ is calculated from Eq. (1). If $dZ/dt>0$, new electrons are added to the system according to the relation

$$\frac{dN_e(t)}{dt} = N\frac{dZ(t)}{dt}, \tag{2}$$

where N_e is the number of electrons and N is the number of atoms per cluster. While the number of electrons changes dynamically with time depending on the laser intensity, the number of ions N_i remains constant, $N_i=N$, and only the corresponding charge states increase according to Eq. (1a). For each new particle, the initial values of the three-dimensional velocity and position must be specified. The initial position is randomly chosen inside the cluster. Since the initial velocity components are not important for the future motion of the particle, they are all assumed to be zero.

The second part of the model deals with the simultaneous motion of the particle ensemble. We consider only ions and unbound electrons; the latter represents both electrons that reside inside the cluster (inner electrons) and electrons that are located outside the cluster (outer electrons). We are particularly interested in modeling the outer electrons, since in

Refs. [19,20] it was surmised that the inner shell ionization yielding the population inversion occurs due to impact with high-energy outer electrons.

The trajectories of the electrons and ions are governed by the relativistic equation of motion

$$\frac{d\vec{p}_i}{dt} = q_i[\vec{E}(t) + \vec{v}_i \times \vec{B}(t)/c] - \sum_j \nabla \Phi_{ij}, \tag{3}$$

$$\vec{p}_i = \gamma_i m_i \vec{v}_i, \quad \gamma_i = 1/\sqrt{1 - |\vec{v}_i|^2/c^2}, \tag{4}$$

$$\frac{d\vec{r}_i}{dt} = \vec{v}_i, \tag{5}$$

where $\vec{p}_i = p_i(x,y,z)$ is the relativistic momentum, γ_i is the relativistic factor, $\vec{r}_i = r_i(x,y,z)$, $\vec{v}_i = v_i(x,y,z)$, m_i and q_i are the coordinate, velocity, mass, and charge of the ith particle, respectively, $|\vec{v}_i|$ is the magnitude of the particle velocity, $\vec{E}$ and $\vec{B}$ are the externally applied electric and magnetic fields, and $\Phi_{ij} = q_i q_j / |\vec{r}_i - \vec{r}_j|$ is the interaction potential between particles i and j (regularization at small $|\vec{r}_i - \vec{r}_j|$ can be adopted from Ref. [24]). Equations (3)–(6) account for relativistic effects, which become important at intensities above 10^{18} W/cm^2. Each particle velocity as well as position is advanced in time according to Eqs. (3)–(5). Since, at any given time, the electron and ion positions and velocities are known, the relativistic momentum can be computed from Eq. (4) and the corresponding macroscopic parameters can be computed. For example, the average electron excursion with respect to the ion core in the direction parallel to the applied electric field, i.e., the dipole moment, can be calculated. The number of electrons inside and outside the cluster can also be tracked. Other quantities of interest, which can be readily derived, are the electron and ion energy distribution functions. The electron energy distribution function $f(E)$ is defined as the fraction of electrons with energies between $E - \Delta E/2$ and $E + \Delta E/2$, divided by a square root of the energy, and has the normalization $\int_0^\infty E^{1/2} f(E) dE = 1$. Since the particle energies are discrete, we count the number of electrons in the energy interval ΔE. We choose ΔE to be one hundredth of the maximum particle energy.

Of particular interest is the energy balance of the system. By multiplying Eq. (3) by $\vec{v}_i$, summing over all species, and integrating in time, one can derive the energy balance equation

$$\sum_i [E_i^{kin}(t) + E_i^{pot}(t)] = \sum_i E_i^{IB}(t), \tag{6}$$

where $E_i^{kin}(t) = \int_0^t \vec{v}_i(t) \cdot [d\vec{p}_i(t)/dt] dt$ and $E_i^{pot}(t) = \int_0^t \vec{v}_i(t) \cdot \Sigma_j \vec{\nabla} \Phi_{ij} dt$ are the ith particle kinetic and potential energy, respectively, and $E_i^{IB}(t) = \int_0^t q_i \vec{v}_i(t) \cdot \vec{E}(t) dt$ is the energy absorbed due to inverse Bremsstrahlung (IB). The total energy absorbed in the system E^{IB} is the right-hand side of Eq. (6).

The symmetry of the system under investigation is important in any physical problem and the presence of symmetry often allows welcome simplifications. In the laser-cluster interaction, the symmetry issue is complicated due to the presence of the magnetic field. If the contribution of the magnetic field in Eq. (3) is small, only two directions need to be considered: parallel and perpendicular to the laser electric field; the analysis can be considered as two dimensional. In the opposite case of sufficiently high magnetic field, the magnetic field deflects the electrons from their trajectory and the analysis becomes fully three dimensional.

III. RESULTS AND DISCUSSION

A. Cluster dynamics at different peak laser intensities

The molecular dynamics model was employed to study the dynamics of small Xe clusters irradiated by a KrF laser with wavelength $\lambda = 248$ nm at high peak intensities, specifically, from 10^{17} to 10^{21} W/cm^2. Our study is relevant to the experiments discussed in Refs. [4,5]. The cluster is assumed to be spherically symmetric and spatially uniform. The cluster size is much smaller than the wavelength λ; hence we consider the electric and magnetic fields as spatially uniform [1,2]. Thus the direction of the electromagnetic fields changes in time, but not in space. The direction of electromagnetic propagation is taken along the y axis; the corresponding laser electric and magnetic fields are parallel to the axes x and z, respectively, namely, $\vec{E} = (E_x(t), 0, 0)$ and $\vec{B} = (0, 0, B_z(t))$. The electric field strength is given by the form $E_x(t) = E_0(t)\cos(\omega t)$. The induced magnetic field is very small compared to the laser magnetic field and has been neglected. For the purpose of clarifying the mechanisms driving the cluster dynamics, the peak laser intensity I_0 is kept constant. This simplification reflects the actual experimental conditions in Refs. [4,5] under which the front of the laser pulse is very steep. Xenon clusters with an initial radius $R_0 = 20$ Å (393 atoms per cluster) are considered. A single cluster located at the origin of the coordinate system is modeled; therefore boundary conditions are not imposed. To account for the impact of neighboring clusters, we can apply periodic boundary conditions at $x,y,z = \pm 200$ Å with an estimated intercluster distance of 400 Å. In order to simplify the computations, we used $\sim 10^3$ test particles, $\sim 10\%$ of which are ions. Importantly, it was found that the results obtained were not sensitive to the number of particles. Each particle is assigned an appropriate mass and charge to account for the distribution of particle species. A suitable time step to advance the velocity and position coordinates is $(2-4) \times 10^{-19}$ s, i.e., the temporal resolution is several thousand time steps per laser cycle. In the present simulations the particles are advanced for ten laser cycles (8.27 fs). A typical computation time is a few minutes per laser cycle.

The first set of figures (Figs. 1–3) refers to a peak laser intensity $I_0 = 10^{17}$ W/cm^2. The average cluster charge calculated according to Eq. (1) is $Z - 1 \approx 12$. We follow the sequence of events as the laser is turned on at time $t = 0$. Figure 1 shows the positions of the test particles at equally spaced times. At $t = 0$, all particles (electrons and ions) reside inside the cluster [Fig. 1(a)]. The electron density $n_e(t=0) = 1.4 \times 10^{23}$ cm^{-3} is several times larger than the critical electron density. After the laser is turned on, the electrons are

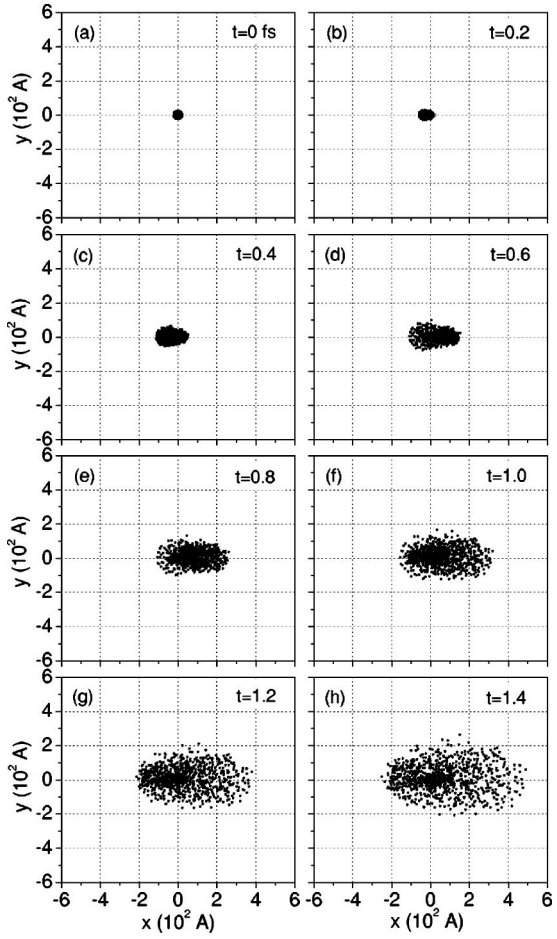

FIG. 1. Positions of the test particles in the *XY* plane at different times. "X" is the parallel to the laser field and "+*Y*" is the direction of propagation. The laser and cluster parameters are $I_0=10^{17}$ W/cm^2, $\lambda=248$ nm, $R_0=20$ Å, $N=393$ atoms/cluster, and $Z=13$. The number of test particles is $\sim 10^3$.

promptly removed from the cluster (outer ionization). We studied the outer ionization by simply counting the number of electrons that leave the cluster. The number of inner electrons decreases exponentially in time with a characteristic time of ~ 0.4 fs. After two laser cycles the strong laser field removes 99% of the electrons from the cluster [Fig. 2(a)]. With most of the electrons outside the cluster, the electron cloud gradually expands due to Coulomb repulsion between the electrons. With only Coulomb forces acting between electrons, the electron cloud would preserve its (nearly) spherical shape. But, as a consequence of the Coulomb attraction between electrons and ions, the electron cloud becomes elongated in the direction of the laser field. At the end of the first laser cycle $t=0.8$ fs [Fig. 1(e)], it has an egglike shape ~ 400 Å long and ~ 200 Å wide. In this state, the electron cloud has dimensions comparable with the intercluster distance; the electron clouds from neighboring clusters overlap and form a (uniform) plasma. The most intriguing observation is the rapid expansion of the electron cloud and the fact that it does not behave as one superparticle as it was surmised in Refs. [19,20]. In fact, we find just the opposite: the electron cloud explodes and creates plasma in less than

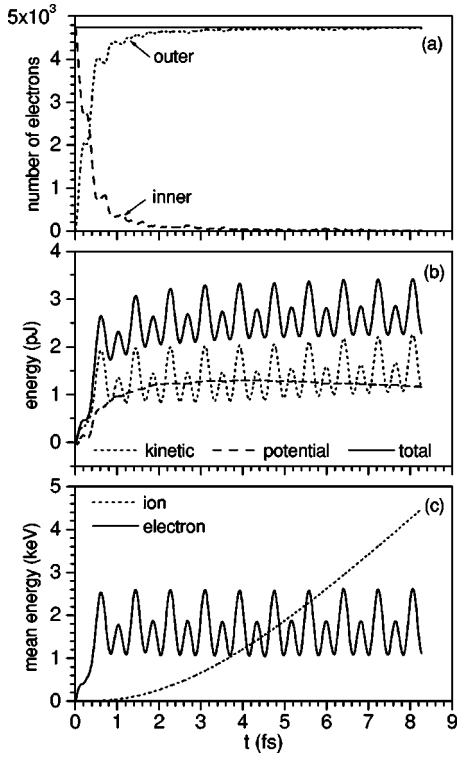

FIG. 2. Number of inner electrons (dashed line), outer electrons (dotted line), and total number of electrons (solid line) (a), kinetic, potential, and total energy (b), and mean electron and ion energy (c) vs time. The conditions are the same as in Fig. 1.

2 fs. This plasma, created as a result of laser-cluster interaction, is very similar to that created in conventional laser-plasma interactions, although two distinct differences exist between them. The first distinction is the "hot" (several keV) plasma created in the laser-cluster interaction, while the laser-plasma interaction generates "cold" electrons with energies of 10–100 eV. The second difference concerns the ions. The laser-cluster interaction results in stripping the cluster of all electrons, thus creating a "giant" ion, consisting of hundreds or thousands of ions, while the laser-plasma interaction creates individual ions. It should be noted, however, that at sufficiently low intensities, both cases produce an average ion charge that is approximately the same.

The energy balance given by Eq. (6) is plotted in Fig. 2(b). The oscillation of the kinetic energy is a result of the constant change of the electron velocity due to the oscillation of the electric field. The potential energy results from the electron and ion cloud separation. The electrons "feel" the pull of the ion core and interact with it. This is also evident from the nonspherical shape of the electron cloud discussed above. The total energy (kinetic plus potential) is equal to the energy absorbed by the cluster due to IB. The cluster absorbs most of its energy during the first laser period, while the electrons are still inside the cluster. The total energy absorbed by the cluster is $E^{IB}=2\times 10^{-12}$ J.

The electron mean energy $\overline{E_e}=\Sigma_{p=e}E_p^{kin}/N_e$ and the ion mean energy $\overline{E_i}=\Sigma_{p=i}E_p^{kin}/N_i$, are plotted in Fig. 2(c). The ion mean energy increases with a rate ~ 0.5 keV/fs. The instantaneous mean electron energy can be considered as a sum of

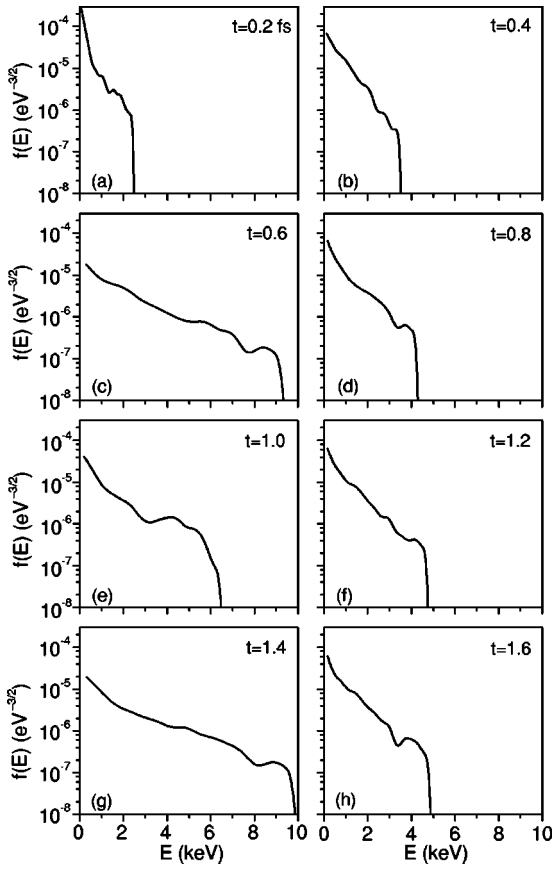

FIG. 3. EEDF at different times. The conditions are the same as in Fig. 1.

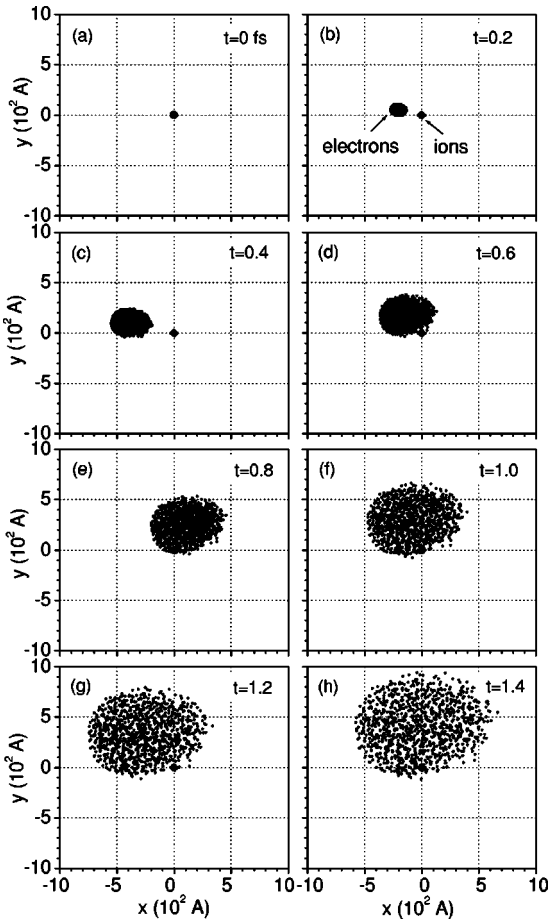

FIG. 4. Positions of the test particles in the *XY* plane at different times. The laser and cluster parameters are $I_0=10^{19}$ W/cm^2, $\lambda=248$ nm, $R_0=20$ Å, $N=393$ atoms/cluster, and $Z=27$.

two energies: "background" energy acquired due to IB ($\sim$1 keV after the first laser cycle) and ponderomotive energy which oscillates in synchronism with the laser field with an amplitude of $\sim$1.2 keV. At the peak laser intensity $I_0=10^{17}$ W/cm^2, they are comparable and the mean electron energy is moderately modulated. This can be examined in detail by studying the electron energy distribution function (EEDF) in Fig. 3. The EEDF is Maxwellian with a temperature varying in time. The cutoff at high energy is attributed to the finite number of particles ($\sim 10^3$) used. At $t=0.4$ fs, the laser field is zero and there is no contribution of the ponderomotive energy to the EEDF. The EEDF consists of "thermal" electrons and is formed by the interplay between heating due to IB and elastic electron-electron collisions. At $t=0.6$ fs, the laser electric field is at its maximum and ponderomotively driven electrons affect the EEDF. Both types of electrons, "thermal" and ponderomotively driven, form the EEDF with a slight prevalence of the thermal ones. The average electron velocity is $(2-3)\times 10^9$ cm/s, i.e., $|v|/c\sim 0.1$ and the electrons may still be considered nonrelativistic. The impact of the magnetic field is small; it changes only slightly the electron trajectories in the direction of the laser propagation.

At the peak laser intensity $I_0=10^{19}$ W/cm^2, the force of the electric field greatly exceeds that of the ion core, a condition that has two important consequences: (i) the electron cloud moves collectively under the action of the laser field (since the attractive force of the ion core is relatively small), and (ii) it retains a spherical shape. The latter seems unusual, but it can be understood as arising from the interplay of forces acting on the electron cloud. On one hand, the electric field is strong enough to exceed the field generated by the ion core. On the other hand, it is small enough to make the contribution of the magnetic field negligible. Thus there are only two dominant forces acting on the electron cloud; they are the laser electric field and Coulomb repulsion between the electrons. The first one leads to a translational motion of the electron cloud in the direction parallel to the field and the second causes a spherically symmetric expansion. One may think of the electron cloud as a moving ball of electrons, slowly expanding in time (Fig. 4). Thus the most prominent feature of the cluster at this laser intensity is the collective behavior of the outer electrons.

Figure 5 is analogous to Fig. 2, but for a peak laser intensity $I_0=10^{19}$ W/cm^2. The potential energy of the system is an order of magnitude smaller compared to the kinetic energy. The kinetic energy oscillates with the laser field, and the total (absorbed) energy follows these oscillations. Figure 5(b) plots the electron and ion kinetic energies. The electron thermal energy absorbed due to IB is only 10–15 keV, while the ponderomotive component is $\sim$120 keV. Since the ponderomotive energy exceeds by far the thermal energy of the electrons, the electron kinetic energy becomes strongly

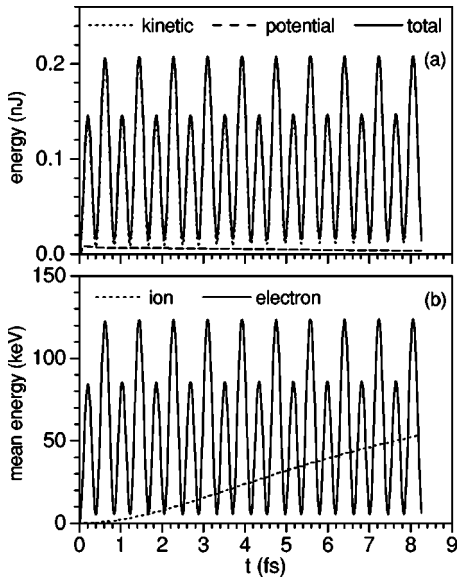

FIG. 5. Kinetic, potential, and total energy (a) and mean electron and ion energy (b) vs time. The conditions are the same as in Fig. 4.

modulated in time. The ion mean energy increases with a rate ~ 5 keV/fs and, at $t=8$ fs, it is near the optimum for the nuclear fusion of hydrogen. The EEDF plotted in Fig. 6 is radically different in comparison to that for the intensity I_0

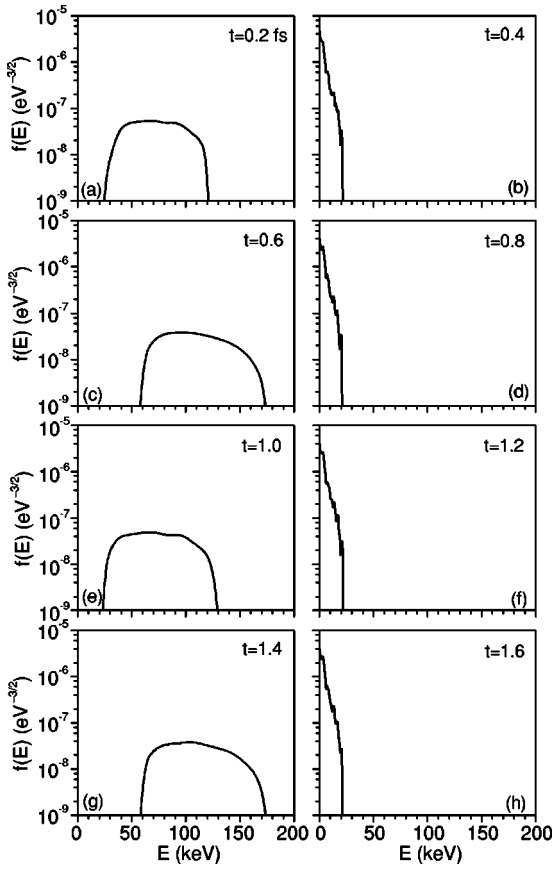

FIG. 6. EEDF at different times. The conditions are the same as in Fig. 4.

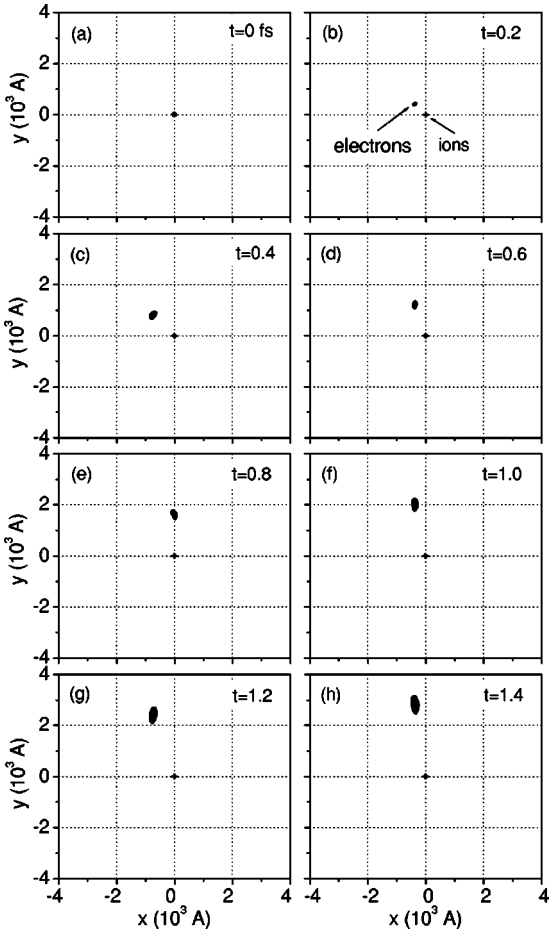

FIG. 7. Positions of the test particles in the *XY* plane at different times. The laser and cluster parameters are $I_0=10^{21}$ W/cm^2, $\lambda=248$ nm, $R_0=20$ Å, $N=393$ atoms/cluster, and $Z=45$.

$=10^{17}$ W/cm^2. At the peak of the laser field, all electrons are accelerated to a very high energy, between 20 and 200 keV. There are practically no electrons with energies below 20 keV. The figures to the right correspond to vanishing electric field and the figures to the left refer to the peak of the laser field. When the laser field is zero, the EEDF is Maxwellian with a temperature of ~ 10 keV. As seen in Fig. 6, the EEDF is transformed dramatically on a time scale of $\sim\frac{1}{4}$ of the laser period. At the peak of the laser field the electron velocities are tightly bunched with $|v|\approx(1-2)\times 10^{10}$ cm/s, i.e., the electrons are relativistic. The impact of the magnetic field on the electrons (the $\vec{v}\times\vec{B}/c$ component of the Lorentz force) becomes significant and causes appreciable deflection of the electron trajectories in the direction of the laser propagation.

The transition from a peak laser intensity $I_0=10^{19}$ W/cm^2 to a peak laser intensity $I_0=10^{21}$ W/cm^2 leads to a dramatic change in both the electron trajectories and the shape of the electron cloud. As expected, at this high intensity, the electrons behave collectively. However, the shape of the electron cloud is no longer spherical: the magnetic field stretches the electron cloud in the direction parallel to the magnetic field (Figs. 7 and 8). Only one femtosecond after the laser field is initiated, the size of the electron cloud be-

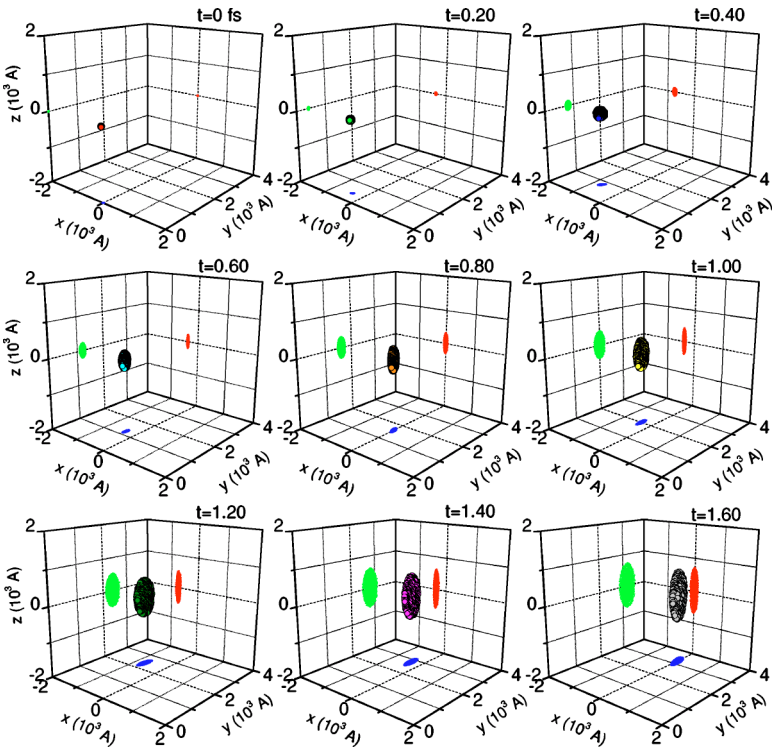

FIG. 8. (Color online) Positions of the test particles at different times. The conditions are the same as in Fig. 7.

comes comparable to the intercluster separation. Indeed, the electromagnetic force acting upon electrons is so large that the electron cloud can reach and hit the next cluster before it expands, closely resembling the "collective oscillation model." The electron cloud trajectory in the direction parallel to the electric field has a triangular shape, a morphology characteristic of the relativistic oscillatory motion of a single electron in an oscillating electric field [Fig. 9(a)]. However, the strong magnetic field orients the electron trajectories in the direction perpendicular to the electric field. The electron velocity is comparable to the speed of light and the force exerted on the electrons by the magnetic field component of the Lorentz force $q_i\vec{v}_i \times \vec{B}/c$ becomes equal to the electric field component of the Lorentz force $q_i\vec{E}$. The electromagnetic field pushes the electrons in the direction of laser propagation and accelerates them to a relativistic velocity. Thus the electrons perform an oscillatory motion in the direction parallel to the electric field (x axis), but in the direction of propagation (y axis), the electrons are accelerated to a relativistic velocity [Fig. 9(a)].

The kinetic, potential, and absorbed energies of the system are plotted in Fig. 9(b). Qualitatively, they look similar to those for $I_0 = 10^{19}$ W/cm^2; the kinetic energy greatly exceeds the potential energy. The temporal evolutions of the electron and ion mean energies are plotted in Fig. 9(c). The ion energy increases quickly with a rate of $\sim$25 keV/fs. The electron thermal energy is $\sim$50 keV, while the ponderomotive energy exceeds 1 MeV and the mean electron energy is strongly modulated. This degree of modulation of the mean electron energy can be explained by comparing the average energy acquired due to IB to the ponderomotive component. The energy acquired due to IB is roughly proportional to the laser field strength, i.e., it scales as $\sim I_0^{1/2}$, while the ponderomotive energy is proportional to the peak laser intensity. That is why at low peak laser intensity ($I_0 < 10^{17}$ W/cm^2) the energy acquired due to IB dominates over the ponderomotive energy and the mean electron energy is only slightly modulated. At peak intensities $I_0 > 10^{17}$ W/cm^2, the energy acquired due to IB is negligible compared to the ponderomo-

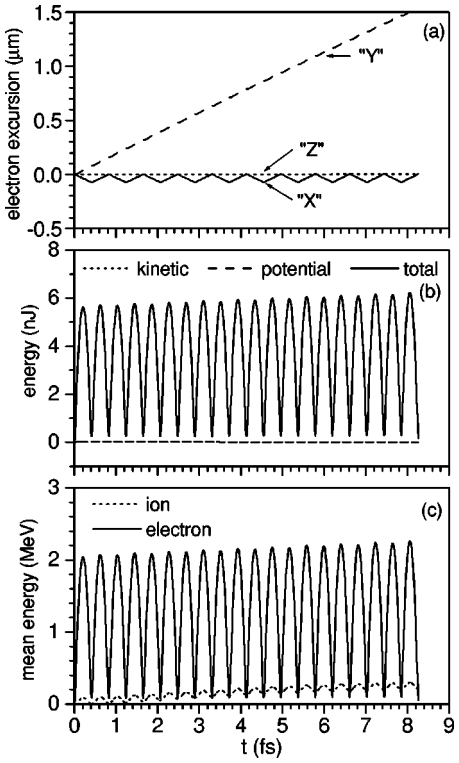

FIG. 9. Electron excursion (a), kinetic, potential, and total energy (b), and mean electron and ion energy (c) vs time. The conditions are the same as in Fig. 7.

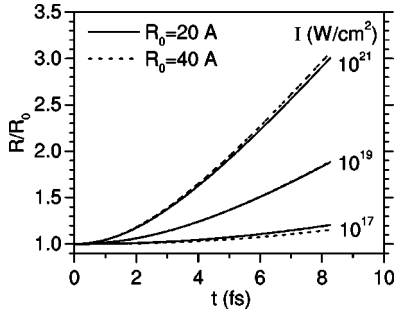

FIG. 10. Normalized cluster size R/R_0 vs time for peak laser intensities $I_0=10^{17}$, 10^{19}, 10^{21} W/cm^2.

tive energy; an outcome that explains the strong modulation of the mean electron energy and EEDF. The transition between these two distinct regimes occurs at a peak intensity $\sim 10^{17}$ W/cm^2 for the wavelength 248 nm.

As discussed by many authors, the cluster slowly expands and disintegrates on a time scale of ~100 fs. We studied the initial stage of the cluster expansion for peak intensities between 10^{17} and 10^{21} W/cm^2. The results for clusters with initial radii of 20 and 40 Å are shown in Fig. 10. The cluster radius $R(t)=\sqrt{2\Sigma_{p=i}\vec{r}_i^2/N}$ is estimated by taking into account the positions of the ions. This expression slightly overestimates the actual radius of the cluster, but it provides a reasonable measure of the expansion. The cluster expansion relative to the initial cluster radius depends primarily on the laser intensity, but not on the initial cluster radius. The mechanisms for cluster expansion are well known. As discussed in Ref. [6], the cluster explosion is due to both the Coulomb repulsion between ions and hydrodynamic forces. If the cluster expansion were solely due to the Coulomb repulsion between ions with mass M and average charge $Z-1$, the expansion would obey the equation [18]

$$\frac{dR}{dt}=\sqrt{\frac{2e^2N(Z-1)}{MR_0}\left(1-\frac{R_0}{R}\right)}. \tag{7}$$

The calculated expansion velocity dR/dt, derived from Fig. 10, is consistent with Eq. (7) for peak intensities between $\sim 10^{17}$ and $\sim 10^{19}$ W/cm^2; we conclude that the cluster expansion is primarily driven by the Coulomb explosion. For a peak intensity $\sim 10^{21}$ W/cm^2, the calculated cluster radius is somewhat larger than that predicted by the analytical formula (7).

B. Collective oscillation model

Now we turn our attention to the collective oscillation model. It requires both the collective motion of the electron cloud and a tightly packed distribution of the electrons with a radius comparable to the initial cluster radius. While at high intensity ($>10^{19}$ W/cm^2) the electrons do behave collectively, the electron cloud necessarily explodes rapidly under internal Coulomb repulsive forces. Note that an increase in the characteristic size of the electron cloud by a factor of 2 means a reduction of the electron density by a factor of 8. The collective oscillation model takes place only if the electron cloud reaches the next cluster before it explodes. That is why our interpretation of the collective oscillation model is slightly different than that in Refs. [19,20]. In our opinion, the electron cloud can only hit a neighboring cluster, not the parent cluster. This is because the magnetic field will deflect the electron trajectory and the electron cloud will "miss" the parent cluster on its way back. This is true even for very short laser wavelengths. Second, the electron cloud can collide with a neighboring cluster only once or twice. The number of interactions is limited by the time the electron cloud explodes (doubles its radius), which is ~0.5 fs. After this time, the electron cloud forms plasma. Let us compare qualitatively the rates for inner-shell ionization of highly charged Xe ions estimated with the collective oscillation model and the "plasma model." The electron density in the collective oscillation model is $\sim 10^3$ times larger compared to the plasma model, which is a significant advantage. However, the duration of the collective oscillation model is only ~0.5 fs, while the plasma model works throughout the laser pulse (typically ~20–50 fs). In addition, the electron cloud can hit a neighboring cluster with certain probability (10–20%). The net result is in favor of the collective oscillation model; its contribution to the inner-shell ionization would be comparable or several times larger than the plasma model. We are not in quantitative agreement with Refs. [19,20], but we are in agreement in principle with the enhancement of the ionization rate in the collective oscillation picture.

C. Electron heating during plasmon resonance

One of the first and most comprehensive models of clusters is that of Ditmire and co-workers [6]. The model assumes that the laser-cluster coupling occurs during the so-called plasmon resonance. This concept, introduced in the modeling of clusters from the very beginning, is widely accepted and used by many. But in a recent study, based on a one-dimensional hydrodynamic model, Milchberg and co-workers [15] argue that the plasmon resonance does not occur due to the high spatial nonuniformity of the cluster.

We have tested the hypothesis of Ditmire using our particle simulation model. Accordingly, a series of runs was conducted at conditions matching those in Ref. [6] ($R_0=50$ Å, $I_0=10^{16}$ W/cm^2, $\lambda=800$ nm). We studied the cluster absorption making computations with different initial electron densities. We started with initial electron density ~20 times higher than the critical density. In the subsequent runs, we gradually reduced it by increasing the initial cluster radius until it became several times smaller than the critical density. We found no enhancement of energy absorption near the plasmon resonance. The most likely reasons are the strongly nonuniform electron density and the time required to establish the polarization of the medium. Also, the polarization in the strong field scenario is not a linear function of the field, but is a nonlinear function. Clusters absorb more energy than gases because the electron and ion densities inside the cluster are much higher than the corresponding densities in the plasma.

IV. SUMMARY

The dynamics of small Xe clusters subject to intense laser radiation using a particle simulation model has been investi-

gated. At a peak intensity exceeding 10^{18} W/cm^2, the problem is clearly of a relativistic nature. All electrons are promptly removed from the cluster in less than two laser cycles. This is true even at a peak intensity $\sim 10^{16}$ W/cm^2. The electron trajectories and the shape of the electron cloud depend on the peak laser intensity. At $I_0 = 10^{17}$ W/cm^2, the motion of the outer electrons is influenced by the ion core and the shape of the electron cloud is not spherically symmetric. At $I_0 = 10^{19}$ W/cm^2, the attractive force of the ion core is negligible compared to the force of the electric field, the electron cloud moves collectively under the action of the laser field, and the electron cloud retains its initial spherical shape. At the highest laser intensity investigated, $I_0 = 10^{21}$ W/cm^2, there is a dramatic transition of the morphology of the electron cloud from a spherical to a "pancake like" configuration that results from the stretching of the electron cloud by the magnetic field. For peak laser intensities $I_0 < 10^{20}$ W/cm^2, the electron cloud expands very rapidly due to Coulomb repulsion between the electrons and forms a plasma. For higher intensities, the electron cloud can be accelerated very quickly and collide with a neighboring cluster before it explodes under internal Coulomb repulsive forces. In this case, it behaves in a manner similar to that envisioned in the collective oscillation model. This is a crucial point for the interpretation of the inner-shell excitation and ionization phenomena discussed in Refs. [19,20].

The mean electron energy and the EEDF are modulated due to ponderomotively driven electrons. The modulation is negligible at sufficiently low laser intensities ($\sim 10^{17}$ W/cm^2) and the instantaneous mean electron energy is equal to the energy the electrons acquire on average from IB. At a sufficiently high laser intensity ($\sim 10^{19}$ W/cm^2), the outcome is reversed; both the mean electron energy and the EEDF are strongly modulated.

The presence of an enhanced heating during the so-called plasmon resonance was not confirmed. A null effect was found. Absence of this phenomenon, predicted by crude spatially averaged fluid models, is probably a consequence of unrealistic assumptions therein.

The laser-cluster interaction at relativistic laser intensities leads to a Coulomb explosion of the cluster and the production of high-energy (MeV) electrons. High-energy (multi-keV) ions are another leading product of the cluster explosion. Nuclear reactions driven by the Coulomb explosion of clusters and the generation of high-energy (MeV) ions can be expected to be an exciting and expanding field of research.

ACKNOWLEDGMENTS

This work was supported in part by DARPA and in part by ONR through the NRL 6.1 program. The authors are thankful to Dr. J. Verboncoeur from the University of California, Berkeley, for fruitful discussions.

[1] A. McPherson, T. S. Luk, B. D. Thompson, K. Boyer, and C. K. Rhodes, Appl. Phys. B: Photophys. Laser Chem. **57**, 337 (1993).
[2] A. McPherson, T. S. Luk, B. D. Thompson, A. B. Borisov, O. B. Shiryaev, X. Chen, K. Boyer, and C. K. Rhodes, Phys. Rev. Lett. **72**, 1810 (1994).
[3] A. McPherson, B. D. Thompson, A. B. Borisov, K. Boyer, and C. K. Rhodes, Nature (London) **370**, 631 (1994).
[4] A. B. Borisov, X. Song, F. Frigeni, Y. Koshman, Y. Dai, K. Boyer, and C. K. Rhodes, J. Phys. B **36**, 3433 (2003).
[5] A. B. Borisov, J. Davis, X. Song, Y. Koshman, Y. Dai, K. Boyer, and C. K. Rhodes, J. Phys. B **36**, L285 (2003).
[6] T. Ditmire, T. Donnelly, A. M. Rubenchik, R. W. Falcone, and M. D. Perry, Phys. Rev. A **53**, 3379 (1996).
[7] T. Ditmire, K. Shigemori, B. A. Remington, K. Estabrook, and R. A. Smith, Astrophys. J., Suppl. Ser. **127**, 299 (2000).
[8] F. Megi, M. Belkacem, M. A. Bouchene, E. Suraud, and G. Zwicknagel, J. Phys. B **36**, 273 (2003).
[9] J. Liu, R. Li, P. Zhu, Z. Xu, and J. Liu, Phys. Rev. A **64**, 033426 (2001).
[10] P. B. Parks, T. E. Cowan, R. B. Stephens, and E. M. Campbell, Phys. Rev. A **63**, 063203 (2001).
[11] S. V. Fomichev, S. V. Popruzhenko, D. F. Zaretsky, and W. Becker, J. Phys. B **36**, 3817 (2003).
[12] I. Kostyukov and J.-M. Rax, Phys. Rev. E **67**, 066405 (2003).
[13] U. Saalmann and J.-M. Rost, Phys. Rev. Lett. **91**, 223401 (2003).
[14] H. M. Milchberg, S. J. McNaught, and E. Parra, Phys. Rev. E **64**, 056402 (2001).
[15] E. Parra, I. Alexeev, J. Fan, K. Y. Kim, S. J. McNaught, and H. M. Milchberg, J. Opt. Soc. Am. B **20**, 118 (2003).
[16] C. Siedschlag and J.-M. Rost, Phys. Rev. Lett. **93**, 043402 (2004).
[17] C. Rose-Petruck, K. J. Schafer, K. R. Wilson, and C. P. J. Barty, Phys. Rev. A **55**, 1182 (1997).
[18] V. P. Krainov and M. B. Smirnov, Phys. Rep. **370**, 237 (2002).
[19] W. A. Schroeder, F. G. Omenetto, A. B. Borisov, J. W. Longworth, A. McPherson, C. Jordan, K. Boyer, K. Kondo, and C. K. Rhodes, J. Phys. B **31**, 5031 (1998).
[20] W. A. Schroeder, T. R. Nelson, A. B. Borisov, J. W. Longworth, K. Boyer, and C. K. Rhodes, J. Phys. B **34**, 297 (2001).
[21] K. Boyer and C. K. Rhodes, Phys. Rev. Lett. **54**, 1490 (1985).
[22] A. Szöke and C. K. Rhodes, Phys. Rev. Lett. **56**, 720 (1986).
[23] C. K. Rhodes, Science **229**, 1345 (1985).
[24] I. Last and J. Jortner, J. Chem. Phys. **120**, 1336 (2004); **120**, 1348 (2004); **121**, 3030 (2004).
[25] I. Last and J. Jortner, Phys. Rev. A **62**, 013201 (2000).
[26] I. Last and J. Jortner, Phys. Rev. A **60**, 2215 (1999).
[27] M. Eloy, R. Azambuja, J. T. Mendonca, and R. Bingham, Phys. Plasmas **8**, 1084 (2001).
[28] M. Eloy, R. Azambuja, J. T. Mendonca, and R. Bingham, Phys. Scr. **T89**, 60 (2001).
[29] T. Taguchi, T. M. Antonsen, Jr., and H. M. Milchberg, Phys. Rev. Lett. **92**, 205003 (2004).
[30] A. B. Borisov, A. V. Borovskiy, V. V. Korobkin, A. M. Prokhorov, O. B. Shiryaev, X. M. Shi, T. S. Luk, A. McPher-

son, J. C. Solem, K. Boyer, and C. K. Rhodes, Phys. Rev. Lett. **68**, 2309 (1992).
[31] A. B. Borisov, A. V. Borovskiy, O. B. Shiryaev, V. V. Korobkin, A. M. Prokhorov, J. C. Solem, T. S. Luk, K. Boyer, and C. K. Rhodes, Phys. Rev. A **45**, 5830 (1992).
[32] A. B. Borisov, X. Shi, V. B. Karpov, V. V. Korobkin, J. C. Solem, O. B. Shiryaev, A. McPherson, K. Boyer, and C. K. Rhodes, J. Opt. Soc. Am. B **11**, 1941 (1994).
[33] A. B. Borisov, O. B. Shiryaev, A. McPherson, K. Boyer, and C. K. Rhodes, Plasma Phys. Controlled Fusion **37**, 56 (1995).
[34] A. B. Borisov, A. McPherson, B. D. Thompson, K. Boyer, and C. K. Rhodes, J. Phys. B **28**, 2143 (1995).
[35] A. B. Borisov, J. W. Longworth, K. Boyer, and C. K. Rhodes, Proc. Natl. Acad. Sci. U.S.A. **95**, 7854 (1998).
[36] A. B. Borisov, S. Cameron, T. S. Luk, T. R. Nelson, A. J. Van Tassle, J. Santoro, W. A. Schroeder, Y. Dai, J. W. Longworth, K. Boyer, and C. K. Rhodes, J. Phys. B **34**, 2167 (2001).
[37] J. Davis, A. B. Borisov, and C. K. Rhodes, Phys. Rev. E **70**, 066406 (2004).
[38] R. W. Hockney and J. W. Eastwood, *Computer Simulation Using Particles* (IOP Publishing Ltd.,Bristol, 1988), p. 18.